*Korean J. Chem. Eng.*, 40(9), 2159-2164 (2023)
DOI: 10.1007/s11814-023-1522-z

pISSN: 0256-1115
eISSN: 1975-7220

# Synthesis of stabilizer-free small PdAg alloy nanoparticles supported on carbon using a continuous Couette-Taylor reactor with enhanced electrochemical activity toward ethanol oxidation reaction

**Pengfei Jiang*, Jiyu Hyun**, Hyun Su Park**, Suk Ho Bhang**, Woo-Sik Kim*,†, and Taekyung Yu*,†**

*Department of Chemical Engineering, Integrated Engineering Major, College of Engineering, Kyung Hee University, Yongin 17104, Korea
**Department of Chemical Engineering, Sungkyunkwan University, Suwon 16419, Korea
(*Received 18 March 2023 • Revised 16 June 2023 • Accepted 22 June 2023*)

**Abstract**−An organic surfactant/stabilizer plays a critical role in synthesizing small and well-dispersed nanoparticles with large catalytic surface areas. However, a stabilizer typically interferes with the catalytic reaction by forming organic layers on the surface of nanoparticles. Here, we report that the role of a stabilizer can be replaced by the periodic and uniform fluid shear of Taylor vortex flow. Small, well-dispersed PdAg alloy nanoparticles on carbon were synthesized in the continuous Couette-Taylor (CT) reactor in the absence of a stabilizer. The synthesized PdAg nanoparticles ($Pd_{64}Ag_{36}$/C) showed two times higher mass activity than commercial Pd/C and good stability (retained 33% after 3,600 s) toward the electrochemical ethanol oxidation reaction due to their clean surface and alloy structure.

Keywords: Catalysts, Couette-Taylor Reactor, Ethanol Oxidation Reaction, PdAg Alloy Nanoparticles, Taylor Vortex Flow

## INTRODUCTION

Direct alcohol fuel cells are one of the most promising energy conversion devices owing to high energy conversion efficiency and good environmental sustainability [1-5]. Palladium (Pd), a precious metal, is considered an efficient anode catalyst in direct alcohol fuel cells for the electrochemical ethanol oxidation reaction (EOR) in alkaline solutions due to weaker CO poisoning during catalytic process [6-8]. The following mechanisms are commonly acknowledged as governing the process of EOR on Pd catalysts [9]:

$$Pd+CH_3CH_2OH+3OH^- \rightarrow Pd-(CH_3CO)_{ads}+3H_2O+3e^-$$
$$Pd+OH^- \rightarrow Pd-OH_{ads}+e^-$$
$$Pd-(CH_3CO)_{ads}+Pd-OH_{ads} \rightarrow Pd-CH_3COOH+Pd$$
$$Pd-CH_3COOH+OH^- \rightarrow Pd+CH_3COO^-+H_2O$$

It is well known that Pd exhibits a limited adsorption capacity for OH, which restricts the reaction rate between $Pd-OH_{ads}$ and $Pd-(CH_3CO)_{ads}$. An effective solution to improve the electrocatalytic activity of Pd is alloying it with oxophilic secondary metals, such as Ag, into bimetallic counterparts [10]. The incorporation of secondary oxophilic metals weakens the affinity of poisoning intermediates and facilitates the adsorption of OH for removing the poisoning intermediates. Although there have been numerous achievements, their practical applications are still less because of the limitations in designing high-performance electrocatalysts for EOR. The structure, composition, size, and dispersion of nanocatalysts are critical for catalytic performance [11-16]. Particularly, the small size of nanoparticles can directly provide more active sites due to a high surface area. Organic stabilizers/surfactants are used to synthesize small nanoparticles by adsorption of the substrates on the surface to restrict particle growth. However, these organic layers block the active sites on the surface and reduce the catalyst activity [17]. There are different methods to remove the stabilizer/surfactant present on the surface of nanoparticles: heat treatment, acid washing, and electrochemical detaching [18,19]. These approaches could change the size or morphology of nanoparticles, which reduces catalytic properties. It is essential to develop an effective approach to synthesize small, well-dispersed nanocatalysts devoid of organic species with high catalytic efficiency.

Recently, fluidic reactors have been considered an alternative way to synthesize small-sized nanoparticles [20]. Taylor vortex flow (TVF) is generated in a continuous Couette-Taylor (CT) reactor, which consists of a rotating inner cylinder and a stationary outer cylinder [21]. This flow creates a periodic toroidal circular motion within the CT reactor, providing effective mixing, high shear stress, and a uniform fluid shear field. It has been reported that effective mixing in the CT reactor can induce high supersaturation and promote nucleation, leading to the production of small particles [22]. Furthermore, the constant and uniform fluid shear field can prevent the aggregation of particles, resulting in well-dispersed particles devoid of unwanted organic species [23]. Thus, TVF has been exploited to synthesize well-dispersed nanoparticles with a clean surface [24].

We have developed a facile route to synthesize well-dispersed alloy nanoparticles without the use of a stabilizer in a continuous CT reactor. Small, surface-clean PdAg alloy nanoparticles well dispersed on carbon were prepared by the continuous operation of the CT reactor. We believe that the periodic and uniform flow pattern of TVF played a critical role in the formation of small $Pd_{64}Ag_{36}$/C alloy

†To whom correspondence should be addressed.
E-mail: wskim@khu.ac.kr, tkyu@khu.ac.kr
Copyright by The Korean Institute of Chemical Engineers.

nanoparticles in the absence of a stabilizer/surfactant. $Pd_{64}Ag_{36}$/C exhibited higher mass activity than commercial Pd/C due to its clean surface and alloy structure.

## MATERIALS AND METHODS

### 1. Materials

Palladium nitrate hydrate ($Pd(NO_3)_2 \cdot xH_2O$), silver nitrate ($AgNO_3$), L-ascorbic acid (99%), polyvinylpyrrolidone (PVP, MW=10,000), potassium hydroxide (KOH), ethyl alcohol ($C_2H_5OH$, 99.5%), Nafion™ 117 containing solution (5%), and commercial palladium on carbon (Pd/C, 10 wt% loading) were purchased from Sigma Aldrich and used without any further treatment. Vulcan XC-72 (carbon) was obtained from Macklin.

### 2. Synthesis of PdAg/C Using a Continuous CT Reactor

Fig. 1 shows a schematic diagram of the CT reactor consisting of two coaxial cylinders: an inner rotating cylinder and an outer stationary cylinder. Table S1 provides the dimensions of the CT reactor: the diameters of the two cylinders and the length of cylinder. Here, $Pd(NO_3)_2 \cdot xH_2O$ and $AgNO_3$ were selected as sources of metal cations. L-ascorbic acid and Vulcan XC-72 were selected as a reducing agent and support, respectively. First, filling distilled water into the CT reactor and heating it to 80 °C using a thermal jacket. Carbon particle suspension (5.0 mg $mL^{-1}$) and an aqueous solution containing metal precursors were separately fed into the CT reactor at different ports of position 1. The concentrations of $Pd(NO_3)_2$ and $AgNO_3$ in the precursor solution were controlled as 2.0/4.0, 3.0/3.0, 4.0/2.0, 4.5/2.1, and 0 mM/6 mM, respectively. The flow rates of the precursor solution and carbon suspension were 2.8 mL $min^{-1}$ and 1.3 mL $min^{-1}$, respectively. L-ascorbic acid aqueous solution (130 mM) was injected into the CT reactor at position 2 with a flow rate of 3.0 mL $min^{-1}$. Thus, the mean residence time (MRT) of the synthetic approach presented was fixed at 2 min. The rotating speed of the inner cylinder was fixed at 1,200 rpm to create toroidal vortices. To achieve a steady state, the product suspension from the outlet port was analyzed after ten-folds of MRT (Fig. S1). PVP-stabilized PdAg/C was synthesized using the same method as that used to synthesize PdAg/C [the concentration of $Pd(NO_3)_2$ and $AgNO_3$ in the precursor solution was 4.0/2.0], except that PVP (1.0 mg $mL^{-1}$) was added to the tank of precursor solution. The product suspension was centrifuged and washed twice with distilled water and once with ethanol. The sample was collected after drying 6 hours at 25 °C in a vacuum oven.

### 3. Characterization

Transmission electron microscopy (TEM), high-resolution TEM (HRTEM) images, high-angle annular dark field-scanning transmission electron microscopy (HAADF-STEM), and energy dispersive X-ray (EDX) STEM mapping images were obtained using a JEM-2100F microscope (JEOL, Japan) operated at 200 kV. The X-ray powder diffraction (XRD) patterns of samples were obtained using a D-MAX/A diffractometer (Rigaku, Japan) at 35 kV and 35 mA. Inductively coupled plasma mass spectrometry (ICP-MS, Leeman, USA) was used to characterize the elemental composition. X-ray photoelectron spectroscopy (XPS) spectra of PdAg/C samples were obtained using a PHI 5000 VersaProbe. The adsorbed species on the surface of PdAg/C were analyzed by Fourier transform infrared (FT-IR) spectroscopy using a Perkin-Elmer Spectrum 100 FTIR (ATR) spectrometer. The loading capacity of PdAg alloy nanoparticles on Vulcan XC-72 was confirmed by using a thermal gravimetric analyzer (TGA, Q5000 IR).

### 4. Electrochemical Measurements

Electrochemical experiments were carried out using a standard three electrode system by a CHI instrument 760E potentiostat (CH Instruments, USA). The glassy carbon electrode (GCE, active geometrical area of ~0.196 $cm^2$) was used as the working electrode, platinum wire as the counter electrode and Ag/AgCl electrode as the reference electrode. All potentials were measured against the Ag/AgCl electrode and converted to the reversible hydrogen electrode (RHE) reference scaled by $E_{(RHE)}=E_{(Ag/AgCl)}+0.197\ V+0.0592\times pH$. The GCE was polished to remove the impurities on the electrode surface by using 0.3 μm and 0.05 μm alumina slurry, respectively, before each measurement. To prepare the catalyst ink, a certain amount

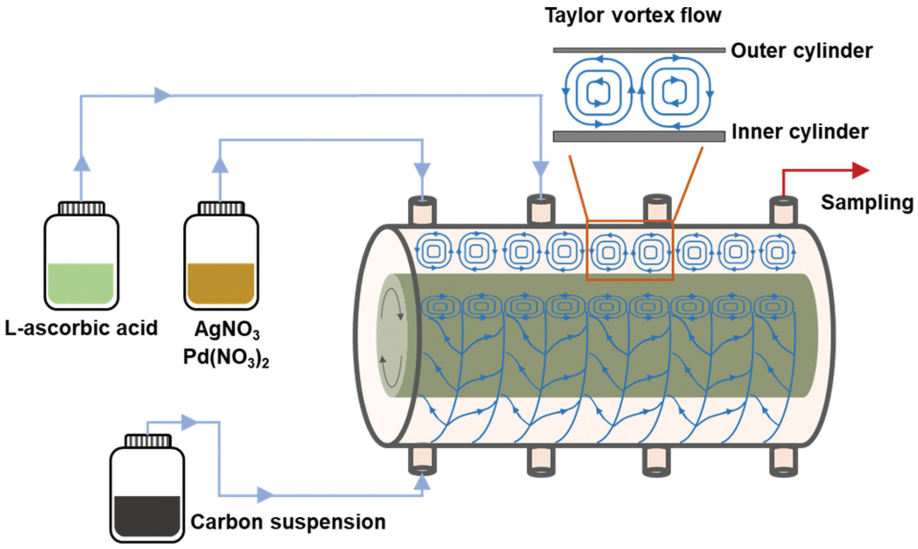



**Fig. 1. Schematic of stabilizer-free PdAg/C catalysts synthesized using a continuous Couette-Taylor reactor.**

of PdAg/C (containing 1 mg of metal catalyst) and 45 μL of Nafion 117 solution were dispersed in 555 μL of ethanol through sonication for 15 min to obtain a homogeneous suspension (the mass concentration was 1.667 mg $mL^{-1}$). The working electrode was prepared by dropping 4.7 μL of catalyst ink onto the surface of GCE and dried at room temperature for 5 min. For comparison, the electrochemical measurements of commercial Pd/C were also carried out under the same conditions. The mass of the metal catalyst on the working electrode was fixed to 40 μg $cm^{-2}$ for all samples. The cyclic voltammetry (CV) measurements were cycled from 0.2 to 1.4 V (vs. RHE) at 50 mV $s^{-1}$ in an $N_2$-saturated 1.0 M KOH solution until a stable CV curve was achieved before EOR measurements. The CV curves of EOR were recorded at a scan rate of 50 mV $s^{-1}$ in an aqueous solution containing KOH (1.0 M) and $C_2H_5OH$ (1.0 M). The mass activity was obtained by normalizing data to the metal mass of one gram. The stability of PdAg/C catalysts was evaluated using chronoamperometry (CA) in a combined solution of 1.0 M $C_2H_5OH$ and 1.0 M KOH for 3,600 s at 0.68 V (vs. RHE).

## RESULTS AND DISCUSSION

PdAg alloy nanoparticles supported on carbon (PdAg/C) were synthesized via chemical reduction in a continuous CT reactor following a previously reported method (Fig. 1) [20]. The rotation speed and MRT were fixed at 1,200 rpm and 2 min, respectively. The atomic ratio of Pd/Ag in nanoparticles was controlled by adjusting the molar ratio of Pd and Ag precursors. Pd : Ag precursor ratios of 1 : 2, 1 : 1, 2 : 1, and 3 : 1 form nanoparticles with Pd : Ag molar ratios of 33 : 67, 49 : 51, 64 : 36, and 74 : 26, respectively, according to the ICP analyses (Fig. 3(a) and Table S2). The molar ratio of Pd/Ag in PdAg/C did not significantly deviate from the initial precursor molar ratio ($Pd_{33}Ag_{67}$/C, $Pd_{49}Ag_{51}$/C, $Pd_{64}Ag_{36}$/C, and $Pd_{74}Ag_{26}$/C). The TEM images of PdAg/C with different molar ratios showed that small nanoparticles were well dispersed on the surface of Vul-

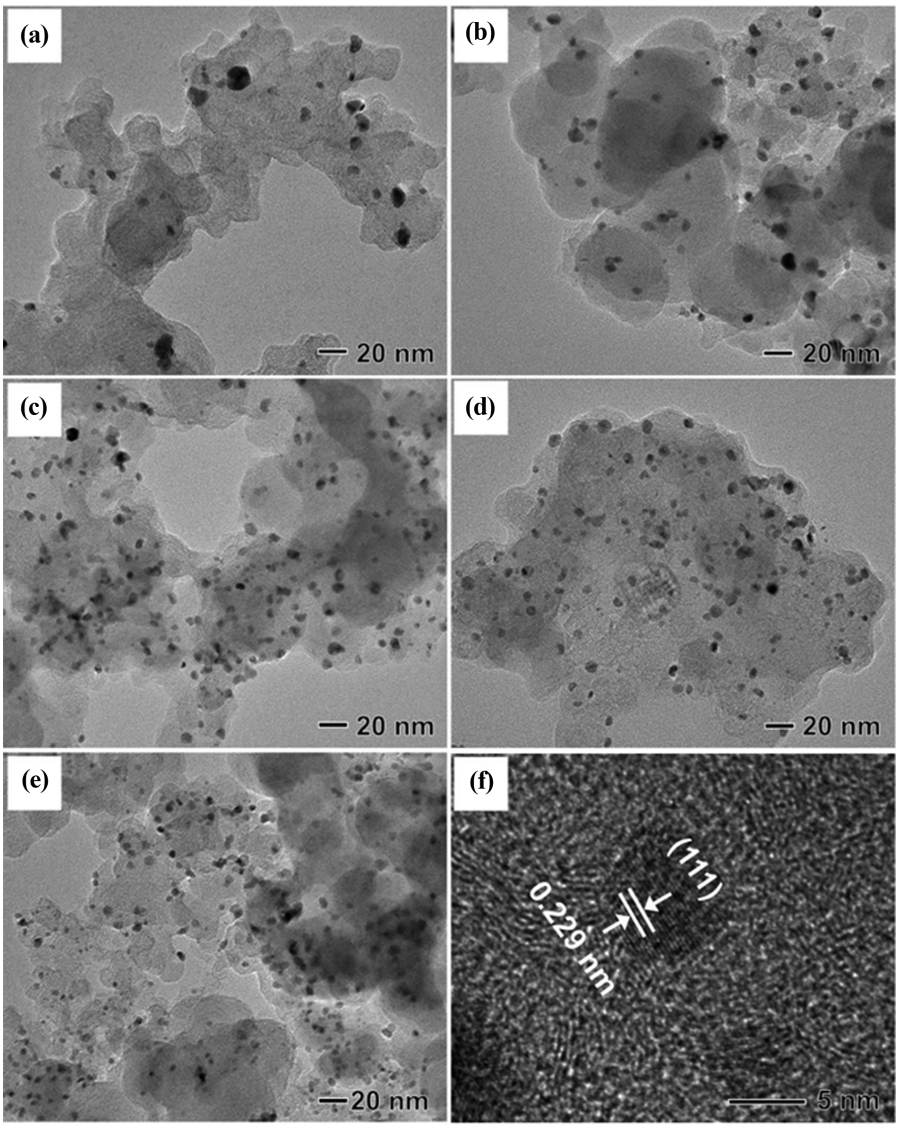



**Fig. 2. TEM images of (a) $Pd_{33}Ag_{67}$/C, (b) $Pd_{49}Ag_{51}$/C, (c) $Pd_{64}Ag_{36}$/C, (d) $Pd_{74}Ag_{26}$/C, and (e) Pd/C synthesized in a continuous CT reactor. (f) HRTEM image of $Pd_{64}Ag_{36}$/C.**

can XC-72 (Fig. 2(a)-(e)). The size of PdAg nanoparticles decreased from 13.2 to 6.4 nm as the concentration of Ag decreased (Fig. S2). This change was due to the incorporation of Ag atoms with larger atomic sizes than those of Pd. Furthermore, HRTEM result revealed that the nanoparticles possessed a highly crystalline single-crystal structure; the measured *d*-spacing was 0.229 nm, which corresponded to the (111) lattice plane of the face-centered cubic structure of the PdAg alloy (Fig. 2(f)). According to TEM and corresponding EDX–STEM elemental mapping analyses, Pd and Ag atoms in PdAg/C catalysts were uniformly distributed on carbon particles, indicating that the as-prepared PdAg nanoparticles were in the alloy phase (Fig. S3). The XRD patterns of the as-prepared PdAg/C and Pd/C showed that the diffraction peaks of all PdAg/C were located between pure Pd (JCPDS 46-1043) and Ag (JCPDS 04-0783), confirming the formation of an alloy structure (Fig. 3(b)) [25,26]. Compared with the Pd/C, the diffraction peaks of PdAg/C shifted to smaller angles with increasing Ag content. This is because when Ag is added to Pd to form an alloy, the larger Ag atoms replace some of the Pd atoms in the crystal lattice. The introduction of larger atoms causes an expansion of the crystal lattice, leading to an increase in the interatomic spacing. Pd $3d_{5/2}$ XPS peaks of the PdAg/C catalysts exhibited higher binding energies compared with those of the commercial Pd/C, suggesting the d-band center of Pd changing by induction of Ag, which was expected to weaken the interactions between the intermediate and the Pd (Fig. 3(c)) [27,28]. FT-IR analysis was performed to detect adsorbed species on the surface of PdAg/C catalysts to prove the clean surfaces of PdAg nanoparticles (without any surfactant/stabilizer) (Fig. 3(d)). PVP-stabilized PdAg/C showed stretching vibration absorption peaks of -C=O (1,661 $cm^{-1}$) and -C-N- (1,298 $cm^{-1}$), which proved the existence of PVP. However, no relevant absorption peaks of PVP were detected in the sample of stabilizer-free PdAg/C catalysts, indicating relative clean surface.

According to our previous report [20,24], TVF in the CT reactor was generated when the rotation speed of inner cylinder exceeded a critical value, resulting in a uniform and periodic flow regime. This plays a crucial role in the synthesis of surface-clean nanoparticles dispersed on carbon particles. The strong toroidal circular fluid motion of TVF effectively micro mixes the reactants, inducing high nucleation in a highly supersaturated state to form small nanoparticles. In addition, the uniform and constant fluid shear stress effectively prevents the aggregation of nanoparticles during the reaction, resulting in the dispersion of nanoparticles on Vulcan XC-72. Therefore, TVF can replace the role of stabilizer to synthesize well-dispersed small nanoparticles on carbon in a continuous CT reactor.

The electrochemical catalytic activities of PdAg/C in the EOR were investigated. For comparison, 8.4 nm-sized PVP-stabilized PdAg/C (Fig. S4, $Pd_{65}Ag_{35}$/C-PVP), Pd/C synthesized in the presence of only the Pd precursor, and commercial Pd/C were introduced as catalysts for the EOR. ~10 wt% of PdAg nanoparticles was maintained on carbon (Fig. S5). We studied their electrochemical performance in a $N_2$-saturated 1.0 M KOH solution (Fig. 4(a)). All

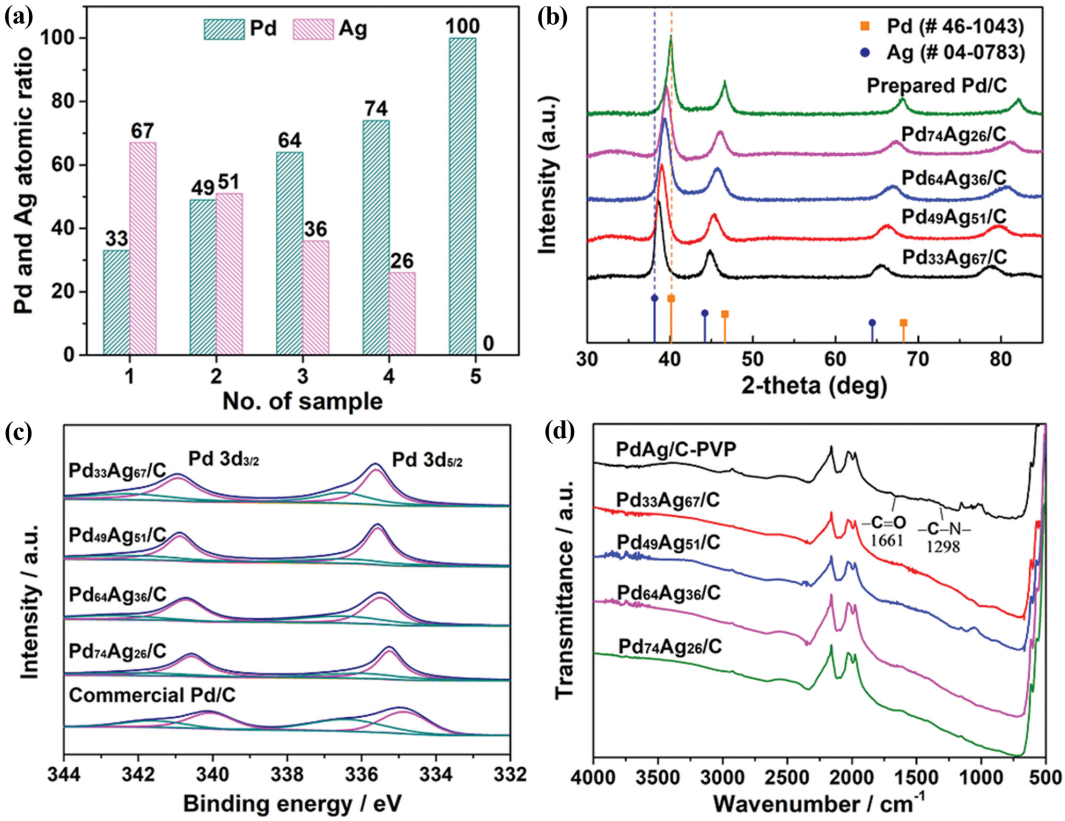



**Fig. 3. (a) Molar ratios of Pd and Ag in PdAg/C determined by ICP-MS. (b) XRD patterns of PdAg/C catalysts. (c) XPS Pd 3d spectra of PdAg/C catalysts and commercial Pd/C. (d) FT-IR spectra of PdAg/C catalysts.**

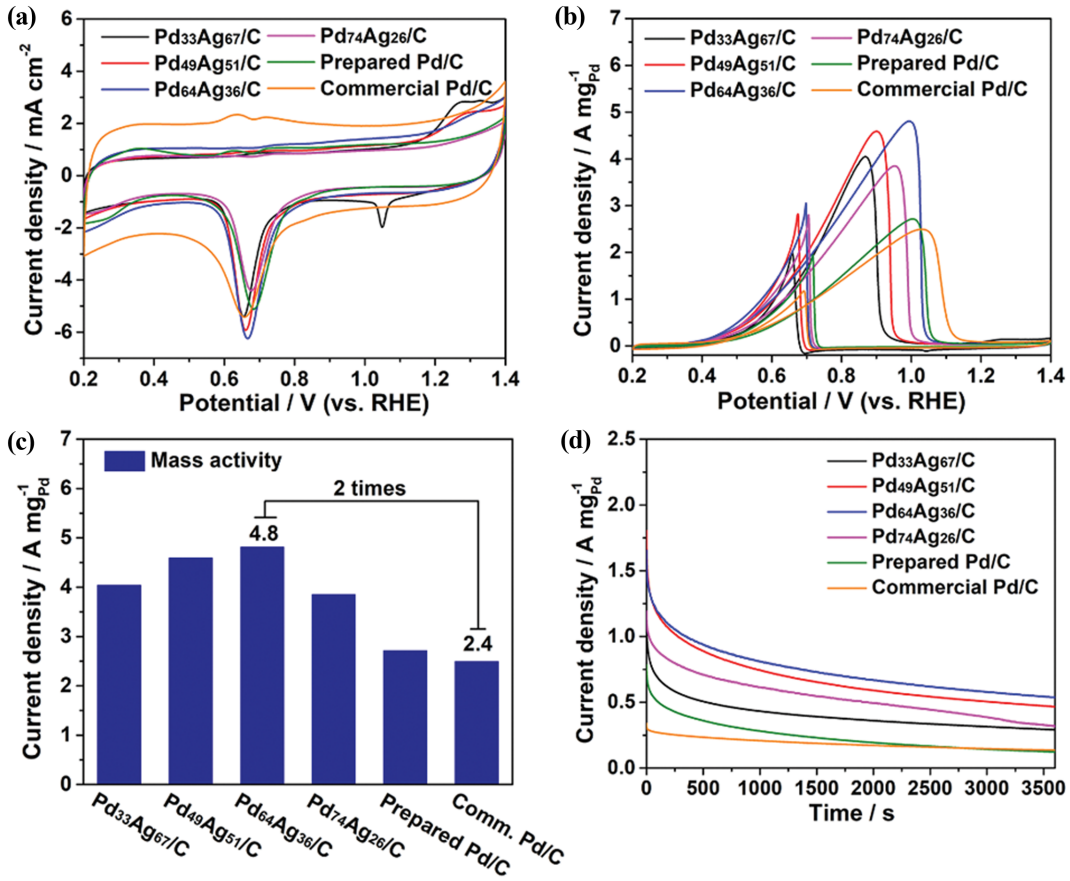



**Fig. 4. Cyclic voltammetry curves of PdAg/C, prepared Pd/C, and commercial Pd/C in (a) 1.0 M KOH and (b) solution containing 1.0 M $C_2H_5OH$ and 1.0 M KOH at 50 mV $s^{-1}$. (c) Mass activities of PdAg/C, prepared Pd/C, and commercial Pd/C. (d) Chronoamperometry curves measured in a solution containing 1.0 M $C_2H_5OH$ and 1.0 M KOH at 0.68 V.**

the samples exhibited a sharp peak within the range of 0.5 to 0.9 V corresponding to the electrochemical reduction of PdO to Pd, indicating that PdAg/C could act as a good electrocatalyst. The EOR performance of PdAg/C was measured from 0.2 to 1.4 V under a $N_2$-saturated solution containing 1.0 M $C_2H_5OH$ and 1.0 M KOH (Fig. 4(b)). The order of the catalytic activity of PdAg/C samples was $Pd_{64}Ag_{36}$/C>$Pd_{49}Ag_{51}$/C>$Pd_{33}Ag_{67}$/C>$Pd_{74}Ag_{26}$/C>prepared Pd/C>commercial Pd/C. The $Pd_{64}Ag_{36}$/C exhibited the highest mass activity (4.8 A $mg^{-1}_{Pd}$), two times higher than that of the commercial Pd/C (2.4 A $mg^{-1}_{Pd}$) (Fig. 4(c)). The mass activity increased as increasing the content of Ag from 0 to 36 wt% in the PdAg alloy nanoparticles, and decreased when the content of Ag was higher than 36 wt%. It suggests that the optimal ratio of Pd/Ag in the PdAg/C catalysts for EOR was 64 : 36 due to alloy composition effect and electronic effect [29]. Ag exhibits remarkable oxophilic behavior, which means it has a strong affinity for oxygen. It readily forms bonds with oxygen and can facilitate the adsorption of oxygen species. Therefore, modulated surface properties induced by Ag introducing would promote the adsorption of reactants and facilitate the transformation of intermediate products, leading to an enhancement in catalytic activity. By contrast, $Pd_{65}Ag_{35}$/C-PVP with a stabilizer on the particle surface to hinder reactivity showed a low mass activity of 1.9 A $mg^{-1}_{Pd}$ (Fig. S6). The mass activity per metal of $Pd_{64}Ag_{36}$/C (3.1 A $mg^{-1}_{PdAg}$) was 1.3 times higher than that of commercial Pd/C (2.4 A $mg^{-1}_{Pd}$) (Fig. S7). Because the size of PdAg nanoparticles in $Pd_{64}Ag_{36}$/C (8.1 nm) is similar to commercial Pd/C (8.3 nm) [30], we believe that the alloying of Pd and Ag will enhance that catalytic activity. Compared to previously reported catalysts, $Pd_{64}Ag_{36}$/C is one of the most active noble metal catalysts (Table S3). Hence, its EOR stability was evaluated using CA in a solution containing 1.0 M $C_2H_5OH$ and 1.0 M KOH for 3,600 s at 0.68 V (Fig. 4(d)). Activity in EOR decreased at a slower rate than that in other catalysts, and mass activity remained constant at 0.54 A $mg^{-1}_{Pd}$ after 3,600 s. By contrast, the mass activity of other catalysts rapidly deceased to 0.12-0.46 A $mg^{-1}_{Pd}$. TEM images indicate that $Pd_{64}Ag_{36}$/C retains its nanostructure, proving its high activity and good stability (Fig. S8).

Based on the above results, a high EOR performance is obtained owing to the clean surface and alloy structure of the synthesized PdAg nanoparticles. A catalyst with a clean surface can provide more active sites and improve catalytic activity. PdAg alloying can effectively enhance the adsorption of OH due to the oxophilicity of Ag. This phenomenon kinetically accelerates the removal of poisoning intermediates [31].

## CONCLUSIONS

We have demonstrated that stabilizer-free well-dispersed PdAg alloy nanoparticles on carbon could be synthesized using the CT

reactor owing to strong uniform fluid shear and effective micro mixing by periodic flow patterns in the reactor. A clean surface and PdAg alloying could impart PdAg/C-enhanced electrochemical properties owing to the EOR. The reported synthetic method has two important advantages in the preparation of electrochemical catalysts: the formation of small and well-dispersed nanoparticles without the use of stabilizers and the ease of preparing alloy nanoparticles. We expect that this method can be used to manufacture various noble metal alloy nanocatalysts.

## ACKNOWLEDGEMENTS

This research was funded by the National Research Foundation of Korea (NRF) under grants listed as NRF-2021R1A5A6002853 and 2020R1A2C1003885. This work was also supported by the Korea Institute for Advancement of Technology (KIAT) and the Ministry of Trade, Industry & Energy (MOTIE) of the Republic of Korea (No. P0017363).

## CONFLICT OF INTEREST

The authors declare that they have no conflict of interest.

## SUPPORTING INFORMATION

Additional information as noted in the text. This information is available via the Internet at http://www.springer.com/chemistry/journal/11814.

## REFERENCES

1. A. K. Choudhary and H. Pramanik, *Korean J. Chem. Eng.*, **36**, 1688 (2019).
2. G. S. Park, S. I. Mo, J. H. Kim and J. W. Yun, *Korean J. Chem. Eng.*, **39**, 1796 (2022).
3. S. H. Kim, H. J. Kim, S. K. Bhatia, R. Gurav, J. M. Jeon, J. J. Yoon, S. Kim, J. Ahn and Y. H. Yang, *Korean J. Chem. Eng.*, **39**, 2156 (2022).
4. Z. Yavari, M. S. Afarani, A. M. Arabi and M. Noroozifar, *Korean J. Chem. Eng.*, **37**, 1669 (2020).
5. S. Barati, M. M. Ghazi and B. Khoshandam, *Korean J. Chem. Eng.*, **36**, 146 (2019).
6. M. Yang, X. Lao, J. Sun, N. Ma, S. Wang, W. Ye and P. Guo, *Langmuir*, **36**, 11094 (2020).
7. N. Ye, Z. Jiang and T. Fang, *Electrochim. Acta*, **352**, 136473 (2020).
8. J. J. Duan, J. J. Feng, L. Zhang, J. Yuan, Q. L. Zhang and A. J. Wang, *Int. J. Hydrog. Energy*, **44**, 27455 (2019).
9. H. Lv, Y. Wang, A. Lopes, D. Xu and B. Liu, *Appl. Catal. B-Environ.*, **249**, 116 (2019).
10. A. L. Wang, X. J. He, X. F. Lu, H. Xu, Y. X. Tong and G. R. Li, *Angew. Chem. Int. Ed.*, **54**, 3669 (2015).
11. A. R. Poerwoprajitno, L. Gloag, S. Cheong, J. J. Gooding and R. D. Tilley, *Nanoscale*, **11**, 18995 (2019).
12. H. Q. Pham, T. T. Huynh, S. T. Nguyen, N. N. Dang and L. G. Bach, *Fuel*, **276**, 118078 (2020).
13. Y. G. Feng, H. J. Niu, L. P. Mei, J. J. Feng, K. M. Fang and A. J. Wang, *J. Colloid Interface Sci.*, **575**, 425 (2020).
14. G. Ren, Z. Zhang, Y. Liu, Y. Liang, X. Zhang, S. Wu and J. Shen, *J. Alloys Compd.*, **830**, 154671 (2020).
15. Z. Tang, L. Zhang, S. Tang, J. Li, J. Xu, N. Li, L. Xu and J. Du, *Nanomaterials*, **12**, 2990 (2022).
16. Z. M. Tang, L. Zhang, J. J. Du and L. J. Xu, *Trans. Nonferrous Met. Soc. China*, **32**, 1994 (2022).
17. Y. Li and M. A. El-Sayed, *J. Phys. Chem. B*, **105**, 8938 (2001).
18. Z. W. Guo, X. W. Kang, X. S. Zheng, J. Huang and S. W. Chen, *J. Catal.*, **374**, 101 (2019).
19. Z. Yin, D. F. Gao, S. Y. Yao, B. Zhao, F. Cai, L. L. Lin, P. Tang, P. Zhai, G. X. Wang, D. Ma and X. H. Bao, *Nano Energy*, **27**, 35 (2016).
20. P. Jiang, W. S. Kim and T. Yu, *ACS Appl. Nano Mater.*, **6**, 1880 (2023).
21. Z. M. Tang, W. S. Kim and T. K. Yu, *Chem. Eng. J.*, **359**, 1436 (2019).
22. S. Lee, C. H. Lee and W. S. Kim, *J. Cryst. Growth*, **373**, 32 (2013).
23. L. Liu, X. Yang, J. Yang, G. Li, Y. Guo, G. Wang and L. P. Wang, *J. Taiwan Inst. Chem. Eng.*, **131**, 104141 (2022).
24. P. Jiang, W. S. Kim and T. Yu, *ACS Appl. Nano Mater.*, **5**, 9604 (2022).
25. J. J. Lv, S. S. Li, A. J. Wang, L. P. Mei, J. J. Feng, J. R. Chen and Z. J. Chen, *J. Power Sources*, **269**, 104 (2014).
26. X. Y. Qiu, R. P. Zhao, Y. A. Li, Y. W. Tang, D. M. Sun, S. H. Wei and T. H. Lu, *RSC Adv.*, **4**, 57144 (2014).
27. X. Yan, X. Hu, G. Fu, L. Xu, J. M. Lee and Y. Tang, *Small*, **14**, 1703940 (2018).
28. B. Hammer, Y. Morikawa and J. K. Nørskov, *Phys. Rev. Lett.*, **76**, 2141 (1996).
29. W. Huang, X. Kang, C. Xu, J. Zhou, J. Deng, Y. Li and S. Cheng, *Adv. Mater.*, **30**, 1706962 (2018).
30. S. Woo, I. Kim, S. Bong, J. Lee and H. Kim, *J. Nanosci. Nanotechnol.*, **11**, 7412 (2011).
31. W. Huang, X. Kang, C. Xu, J. Zhou, J. Deng, Y. Li and S. Cheng, *Adv. Mater.*, **30**, 1706962 (2018).

# Supporting Information

# Synthesis of stabilizer-free small PdAg alloy nanoparticles supported on carbon using a continuous Couette-Taylor reactor with enhanced electrochemical activity toward ethanol oxidation reaction

**Pengfei Jiang*, Jiyu Hyun**, Hyun Su Park**, Suk Ho Bhang**, Woo-Sik Kim*,†, and Taekyung Yu*,†**

*Department of Chemical Engineering, Integrated Engineering Major, College of Engineering, Kyung Hee University, Yongin, 17104, Korea
**Department of Chemical Engineering, Sungkyunkwan University, Suwon 16419, Korea
(*Received 18 March 2023 • Revised 16 June 2023 • Accepted 22 June 2023*)

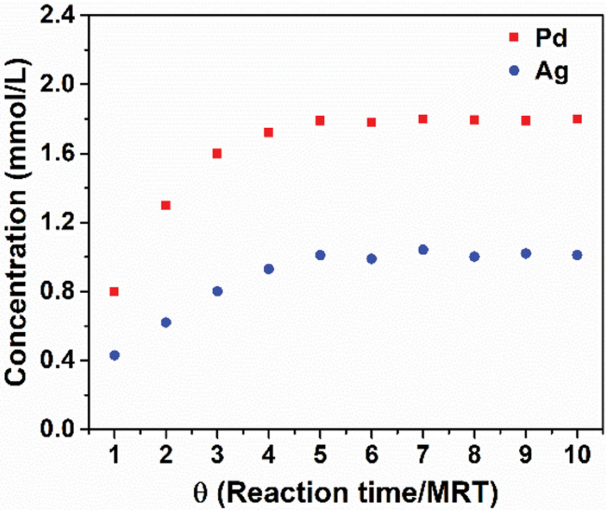



**Fig. S1. ICP analysis results of $Pd_{64}Ag_{36}$/C prepared in a continuous CT reactor obtained at different reaction times.**

**Table S1. Geometric parameters of the Couette-Taylor reactor used in the present synthesis**

| Parameters | |
|---|---|
| Radius of outer cylinder ($r_o$) | 20.78 mm |
| Radius of inner cylinder ($r_i$) | 20.00 mm |
| Length of inner cylinder (L) | 120 mm |
| Gap size (d) | 0.78 mm |
| Working volume (V) | 12.2 mL |

**Table S2. ICP-MS test results of Pd and Ag with different ratios**

| Ideal molar ratio of Pd/Ag | ICP analysis result | | Real molar ratio of Pd/Ag |
|---|---|---|---|
| | Pd (ppm) | Ag (ppm) | |
| $Pd_1Ag_2$ | 91.3 | 194 | $Pd_{33}Ag_{67}$ |
| | 92.0 | 193 | |
| | 91.7 | 194 | |
| $Pd_1Ag_1$ | 153 | 163 | $Pd_{49}Ag_{51}$ |
| | 153 | 163 | |
| | 153 | 163 | |
| $Pd_2Ag_1$ | 191 | 108 | $Pd_{64}Ag_{36}$ |
| | 192 | 108 | |
| | 190 | 109 | |
| $Pd_3Ag_1$ | 243 | 86.8 | $Pd_{74}Ag_{26}$ |
| | 242 | 87.2 | |
| | 242 | 86.7 | |
| Pd | 289 | | Pd |
| | 288 | | |
| | 290 | | |

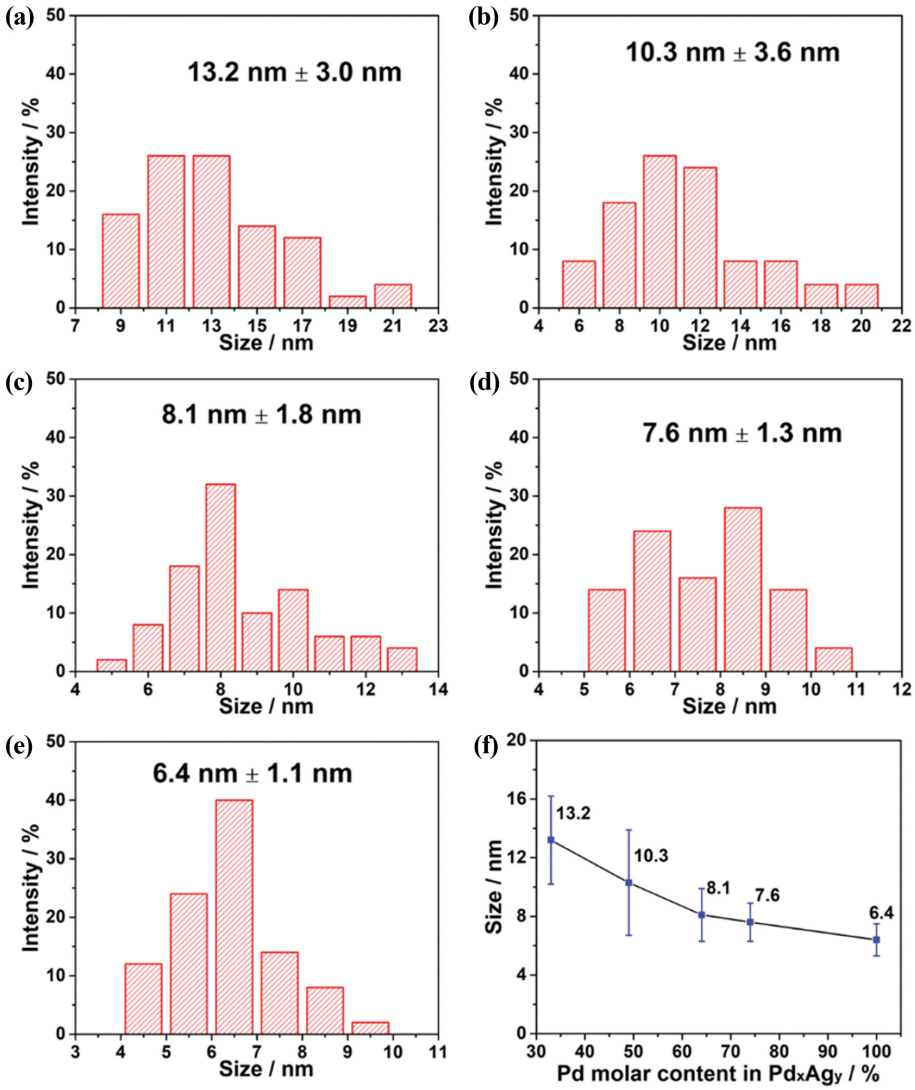



**Fig. S2. Size distributions of (a) $Pd_{33}Ag_{67}$/C, (b) $Pd_{49}Ag_{51}$/C, (c) $Pd_{64}Ag_{36}$/C, (d) $Pd_{74}Ag_{26}$/C, and (e) Pd/C synthesized in a continuous CT reactor. (f) Size change of the PdAg nanoparticles on carbon.**

**Table S3. Comparison of $Pd_{64}Ag_{36}$/C catalyst with the previous reported catalysts for the ethanol oxidation reaction**

| Catalyst | Peak current density ($A\ mg_{Pd}^{-1}$) | Electrolyte solution | Reference |
|---|---|---|---|
| Pd@PdAg/C | 2.52 | 1.0 M $C_2H_5OH$+1.0 M KOH | [1] |
| PdAg nanodendrites | 2.6 | 1.0 M $C_2H_5OH$+1.0 M KOH | [2] |
| PdAg@Pd networks | 3.48 | 1.0 M $C_2H_5OH$+1.0 M KOH | [3] |
| PdAg nanoparticles | 2.43 | 1.0 M $C_2H_5OH$+1.0 M KOH | [4] |
| PdAg/$CeO_2$/C | 4.94 | 1.0 M $C_2H_5OH$+1.0 M KOH | [5] |
| PdAg/MWCNT | 1.62 | 1.0 M $C_2H_5OH$+1.0 M KOH | [6] |
| PdAg Nanoflowers | 1.61 | 1.0 M $C_2H_5OH$+1.0 M KOH | [7] |
| $Pd_{64}Ag_{36}$/C | 4.8 | 1.0 M $C_2H_5OH$+1.0 M KOH | This work |

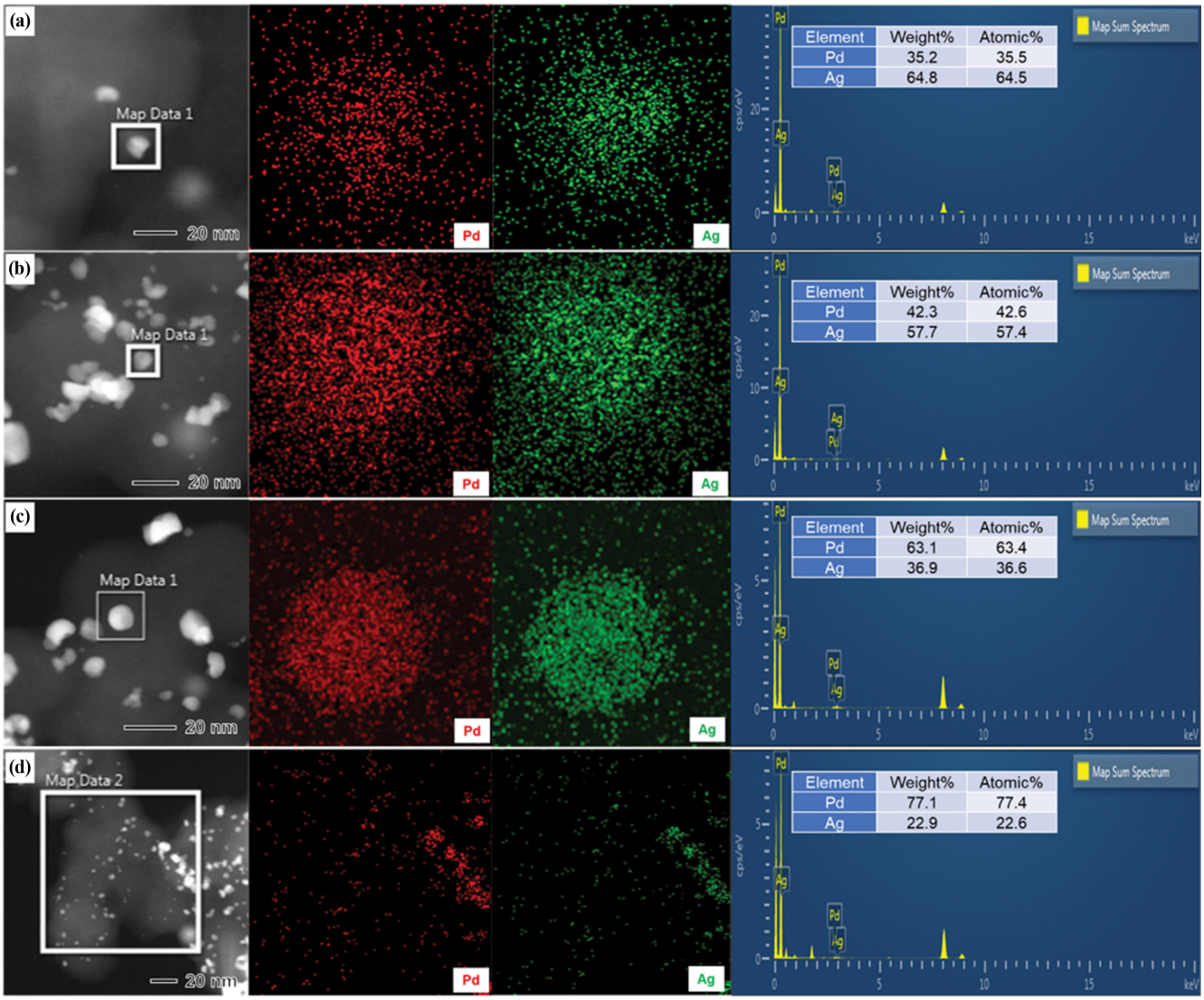



Fig. S3. HAADF-STEM image EDS mapping images of (a) $Pd_{33}Ag_{67}$/C, (b) $Pd_{49}Ag_{51}$/C, (c) $Pd_{64}Ag_{36}$/C, and (d) $Pd_{74}Ag_{26}$/C.

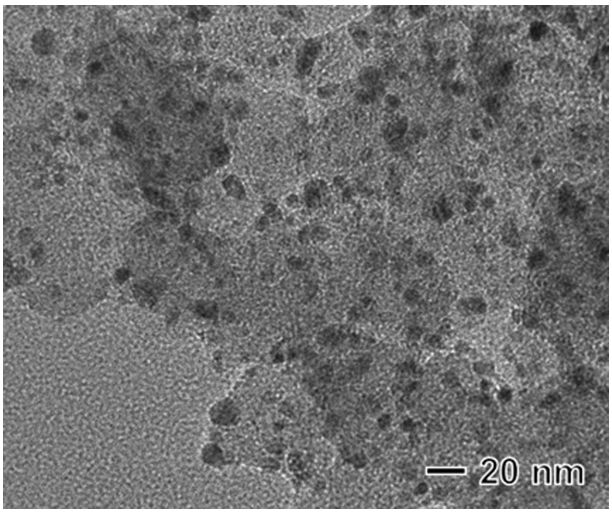



Fig. S4. TEM image of $Pd_{65}Ag_{35}$/C-PVP.

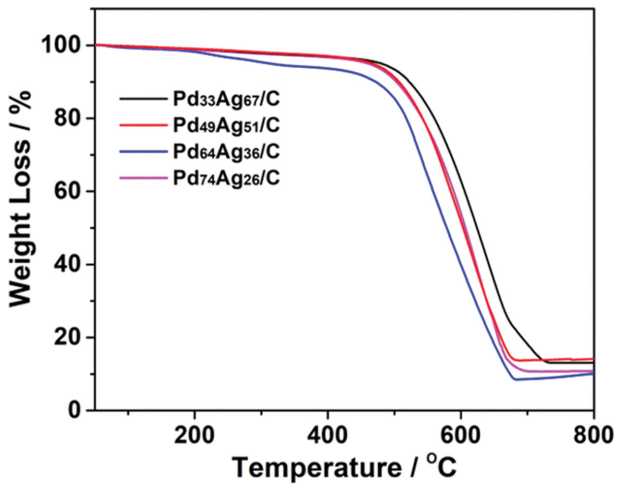



Fig. S5. TGA curves of PdAg/C catalysts prepared in a continuous CT reactor.

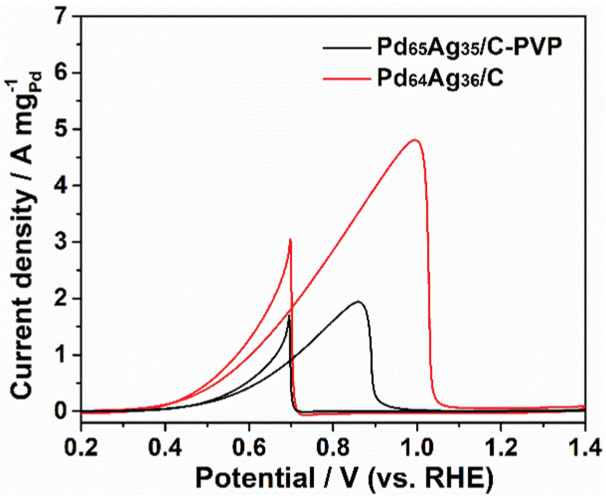



**Fig. S6. Cyclic voltammetry curves of the $Pd_{65}Ag_{35}$/C-PVP and $Pd_{64}Ag_{36}$/C in 1.0 M $C_2H_5OH$+1.0 M KOH at 50 mV $s^{-1}$.**

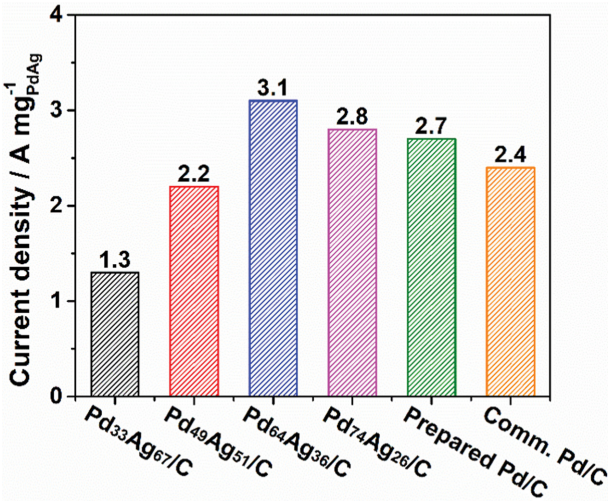



**Fig. S7. Mass activities of the PdAg/C, prepared Pd/C, and commercial Pd/C after normalization to mass of PdAg.**

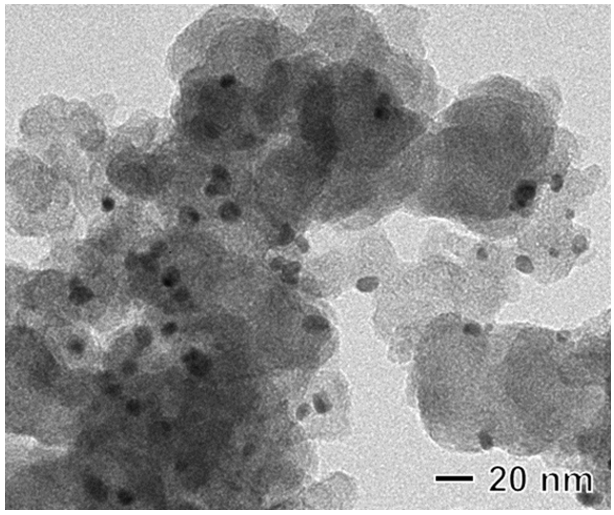



**Fig. S8. TEM image of the $Pd_{64}Ag_{36}$/C after the stability test.**

## REFERENCES


1. J. Huang, Q. Liu, Y. Yan, N. Qian, X. Wu, L. Ji and H. Zhang, *Nanoscale Adv.*, **4**, 111 (2022).
2. W. Huang, X. Kang, C. Xu, J. Zhou, J. Deng, Y. Li and S. Cheng, *Adv. Mater.*, **30**, 1706962 (2018).
3. H. You, F. Gao, T. Song, Y. Zhang, H. Wang, X. Liu and Y. Du, *J. Colloid Interface Sci.*, **574**, 182 (2020).
4. J. Chen, M. Yang, M. Pang, F. Gao and P. Guo, *Colloids Surf. A Physicochem. Eng. Asp.*, **629**, 127404 (2021).
5. A. Xie, Q. Zhang, H. He and C. Peng, *New J. Chem.*, **44**, 17761 (2020).
6. A. M. M. Adam, M. Deng, A. Zhu, Q. Zhang and Q. Liu, *Electrochim. Acta*, **339**, 135929 (2020).
7. D. Bin, B. Yang, K. Zhang, C. Wang, J. Wang, J. Zhong and Y. Du, *Chem.-A Eur. J.*, **22**, 16642 (2016).